Electron-atom interactions in a resonant optical enhancement cavity

Martyn Hussey, Sarah Jhumka, and Andrew James Murray[*]

Photon Science Institute, School of Physics and Astronomy, University of Manchester, Manchester, M13 9PL, United Kingdom

An experiment is described that studies electron collisions with laser-excited atoms inside a resonant optical enhancement cavity. A confocal cavity is used to significantly increase the laser power at the interaction region, so that experiments become possible with low-power continuous-wave lasers, particularly at blue and UV wavelengths. The increased power inside the cavity allows previously inaccessible targets and states to be investigated. The method is tested using superelastic scattering experiments from laser-excited calcium at 423 nm for an electron energy of 45 eV, and data are presented at 100 eV using the enhancement cavity.

PACS number(s): 34.80.Dp

I. INTRODUCTION

The very high coherence radiation deliverable from tunable continuous-wave (CW) lasers has become a powerful tool for manipulation of atoms in modern atomic physics. This radiation is used to selectively control both internal and external states of an atomic ensemble, leading to the experiments and techniques we describe here. These include laser cooling and trapping, manipulation of atoms onto surfaces, quantum coherence studies, and time-reversal collision experiments, to name a few. In these types of experiments the wavelength of the radiation is controlled to better than 1 part in 10^9, which is possible with modern ring and external cavity diode laser systems.

Recent advances in laser development have expanded the wavelength range of tunable CW lasers. The most powerful are dye and Ti:sapphire ring lasers, which can deliver radiation from $\sim$400 to $\sim$1100 nm, with output powers up to 4 W at the peak of their gain. External frequency doublers extend this range down to $\sim$210 nm, although their output may be only a few milliwatts in the deep UV. As such, it is very difficult to carry out experiments that require both high-resolution radiation and high power in this wavelength regime.

The technique described here overcomes these difficulties by placing a stabilized, resonant optical enhancement cavity around the interaction region so as to increase the laser power interacting with the atomic ensemble. In essence, the cavity redirects unused laser radiation back through the interaction region so that the intracavity power increases. Intracavity losses due to scattering by the atoms and at the mirror surfaces, and due to transmission out of the cavity at the mirrors, define the overall enhancement in the steady state. Under *impedance matching* conditions, the transmission of the input coupler is adjusted to maximize the intracavity power by considering all losses. The condition for maximum power transfer into the cavity depends upon the type of cavity that is used. In general, all cavity mirrors (apart from the input coupler) have as high a reflectivity r as possible and should have low scattering losses. Under these conditions, attenuation of the intracavity field due to spontaneous emission from the atomic ensemble located inside the cavity primarily controls the power gain that is possible.

Several different cavity arrangements can be adopted, ranging from standing-wave cavities through to more complex delta and bow-tie traveling wave designs. In the present experiments a two-mirror confocal cavity was chosen, as this configuration can be installed directly into the laser beam path inside the superelastic electron spectrometer. Further, the confocal design preserves the polarization of the incident radiation to the cavity field, which is important for experiments that are critically sensitive to the direction of the field (as are the superelastic scattering experiments described here). Confocal cavities require the mirror spacing L_C to be equal to the radius of the curvature of the mirrors. In the experiments detailed here $L_C = 150$ mm was chosen, as suitable mirrors were available commercially [1]. This mirror spacing allowed the cavity to be installed inside the vacuum chamber without significant modification to the existing electron spectrometer.

II. CALCULATION OF THE CAVITY GAIN

In a confocal enhancement cavity a transmitted light ray passes through the atomic beam four times before returning to the input coupler, as shown in Fig. 1. The product of the attenuation in each cycle of the cavity due to the atomic beam is then given by the total round-trip intensity attenuation, $l_{\text{tot}}(t) = l_2 l_4 l_6 l_8$. The attenuation through the atomic beam along each path of a cycle depends on many factors. These include the atomic beam density and size (as set by the operating conditions of the experiment), the intracavity power along the path (which changes with time), detuning from atomic resonance (due, for example, to the Doppler profile of the atomic beam), detuning from cavity resonance (as occurs if the cavity length or laser wavelength alter), the transition lifetime of the excited states coupled by the laser, and the time-varying population of excited and ground-state atoms. The attenuation factors are time dependent, since the population of laser-excited targets varies due to Rabi cycling and spontaneous emission [2], and since the cavity field changes in time after turn-on. The cavity field and atomic ensemble hence form a strongly coupled system. A full solution of the dynamics of the interacting system hence must consider changes in both the intracavity field and atomic ensemble. This is a complex problem that depends on several different experimental parameters. A general theoretical description of

_____

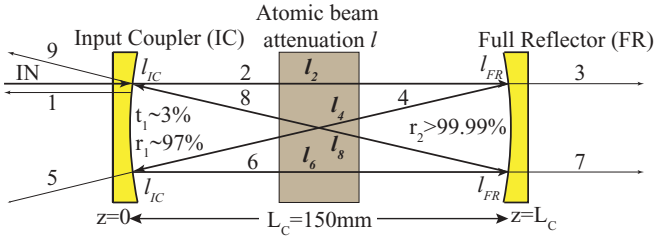[*]Andrew.Murray@manchester.ac.uk

FIG. 1. (Color online) The confocal cavity, consisting of an input coupler (IC, transmission $t_1 \sim 3\%$) and full reflector (FR, reflectivity $r_2 > 99.99\%$) spaced at a distance L_C. Input ray IN passes through IC and traverses a total distance L_{tot} along paths 2,4,6, and 8 before being relaunched into the cavity. Path 1 shows the reflected light from the cavity, whereas paths 3,5,7, and 9 show rays that exit the cavity during a single round trip. Intracavity losses are principally due to attenuation in the atomic beam (represented by attenuation coefficients l_2, l_4, l_6, and l_8), although additional losses may also occur due to scattering from deposition of atoms onto the mirrors (represented by loss terms l_{IC}, l_{FR}).

the dynamics of this coupled system will be presented in a future publication [3].

Additional time-*independent* losses occur at each of the mirrors as a ray cycles around the cavity. These losses arise either from scattering of the laser beam at the mirror surface, or due to leakage of light through the mirrors out of the cavity. In the confocal design adopted here, the input coupler has a reflectivity $r_1 \sim 97\%$ and the full reflector has $r_2 > 99.99\%$, both mirrors having a surface flatness better than $\lambda/10$ at 420 nm. For a complete cycle of the cavity, a ray reflects twice from each mirror and so the round-trip intensity reduces by a factor $r_1^2 r_2^2$. Further losses may arise due to contamination of the mirror surfaces (e.g., by deposition of background atoms from the atomic beam). This unwanted deposition onto the mirrors can be minimized by careful design of the atomic beam oven and the cold trap used to contain the beam after it has passed through the interaction region.

For the experiments presented here, the cavity gain was large enough to ensure the intracavity field reached equilibrium a few hundred nanoseconds after turn-on. Under these *steady-state* conditions, the field in the cavity is stable and unchanging, and so losses from the atomic ensemble no longer depend upon time. For an atomic beam of uniform density, we can then write $l_2 = l_6 = l_2^{SS}$ and $l_4 = l_8 = l_4^{SS}$ under steady-state conditions. The power enhancement inside the cavity can be directly determined by considering how the intracavity field builds-up as a ray cycles between the mirrors. This steady-state enhancement is given by [3]

$$G_{\text{Cav}}^{SS} = \frac{P_{\text{Cav}}^{SS}}{P_{\text{inc}}} = \frac{t_1}{1 + l_2^{SS} l_4^{SS} r_1 r_2 + 2\sqrt{l_2^{SS} l_4^{SS} r_1 r_2} \cos\left(\frac{k L_{\text{Tot}}}{2}\right)}$$

$$\Rightarrow G_{\text{Cav}}^{SS(\text{peak})} = \frac{t_1}{\left(1 - \sqrt{l_2^{SS} l_4^{SS} r_1 r_2}\right)^2}, \qquad (1)$$

where k is the wave number of the incident radiation, L_{Tot} is the total path length of the ray in the cavity, and P_{inc}, P_{Cav}^{SS} are the incident laser power and steady-state cavity power. Losses arising from additional scattering on the mirror surfaces (e.g., from deposition) can be included as fractional reductions

l_{IC}, l_{FR} in the reflection coefficient of each mirror compared to their nominal value, so that r_1 is replaced by $l_{IC} r_1$ and r_2 by $l_{FR} r_2$ in Eq. (1). The peak of the gain profile $G_{\text{Cav}}^{SS(\text{peak})}$ is also given. Impedance matching maximizes $G_{\text{Cav}}^{SS(\text{peak})}$ with respect to the transmission of the input coupler t_1, yielding $t_1^{\text{match}} = 1 - l_2^{SS} l_4^{SS} l_{IC} l_{FR} r_2$ for this type of cavity.

III. EXPERIMENTAL APPROACH

The confocal enhancement cavity was installed in the superelastic scattering chamber [4,5] as shown in Fig. 2. The laser beam (diameter ~ 2 mm) enters the vacuum chamber through a window and passes vertically via a mode-matching lens into the cavity. An oven produces a well-collimated calcium beam at the interaction region [6], where it intersects the intracavity laser beam and an electron beam from the gun. Electrons *superelastically* scattered from laser-excited calcium (i.e., which gain energy) are detected by an analyzer that rotates around the scattering plane. The superelastic electron rates are measured at set scattering angles θ_e as a function of the laser polarization. These rates are used to calculate atomic collision parameters (ACPs) that directly relate to the shape of
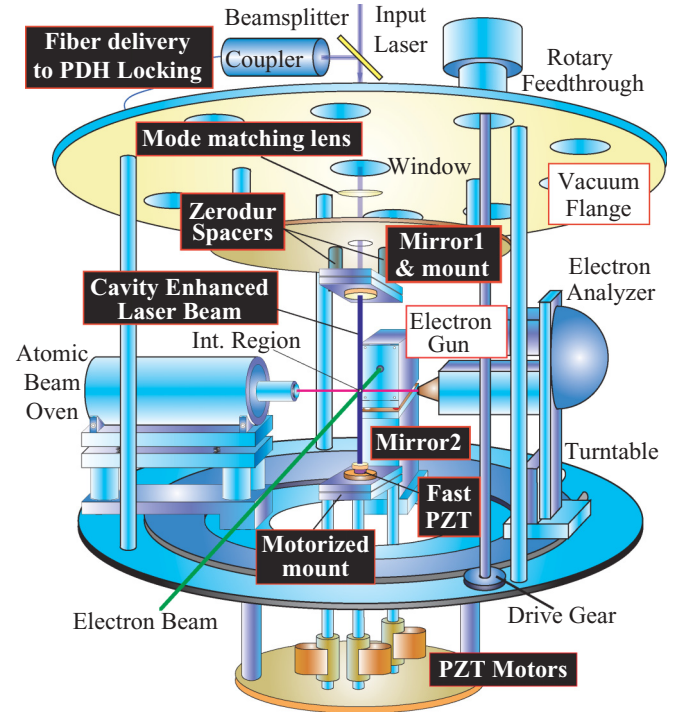

FIG. 2. (Color online) The experimental apparatus, showing the electron spectrometer (gun, oven, and electron energy analyzer), and the confocal optical enhancement cavity (mirrors 1 and 2). The complete assembly is located inside a vacuum chamber pumped by a 300-l/s ion pump during operation. A liquid-nitrogen-cooled cold trap (not shown) is used to capture and confine the atomic beam onto a cold surface after passing through the interaction region. This minimizes unwanted deposition onto cavity mirrors. Reflected light from the cavity is delivered to locking electronics through 10 meters of multimode optical fiber. The cavity length and angle of the full reflector (mirror 2) are controlled by three PZT motors, whereas the locking point is maintained using a fast PZT that controls the axial position of mirror 2.

the atomic charge cloud produced by an equivalent *inelastic* electron collision. The superelastic technique can hence be considered as the time reversal of an inelastic electron-photon coincidence experiment [2–5].

To ensure the cavity spacing was correctly set for maximum gain while the experiment was running, the full reflector (mirror 2) could be adjusted using three externally controlled piezoelectric transducer (PZT) motors. The motors were located ~300 mm below the interaction region on Zerodur rods to reduce any magnetic field they produced to <2 mG at the collision point. The input coupler (mirror 1) was mounted using Zerodur rods so as to minimize any cavity length variation when the oven was heated to the required emission temperature of ~1000 K.

Mirror 2 was fixed to a fast-response piezoelectric (PZT) cylinder that allowed the cavity length to be controlled actively, thereby cancelling the effects of vibration. This was essential to ensure the cavity remained on resonance with the laser beam throughout data collection. The cavity on-resonance condition was maintained using the Pound-Drever-Hall (PDH) technique [7] by monitoring the back-reflected signal from the cavity using a fiber delivery system external to the chamber as shown. The laser was locked to the atomic transition using a feedback system that monitored fluorescence from the interaction region on a split photodiode.

In practice, locking the cavity to the laser frequency was found to be very difficult due to the sensitivity to vibrations from a turbomolecular pump that was used to maintain vacuum. This prevented the PDH control system from locking the cavity onto resonance for extended periods of time, and so an additional 300 l/s ion pump was installed onto the chamber. During data collection the turbo pump was switched off, leaving the ion pump to maintain the vacuum in the spectrometer at ~2 × 10⁻⁷ Torr. This eliminated problems from turbo-pump vibrations and allowed the PDH control system to continuously maintain a lock for several days during data collection.

Figure 3 shows an example of the signal detected from the fiber external to the vacuum chamber as the cavity length
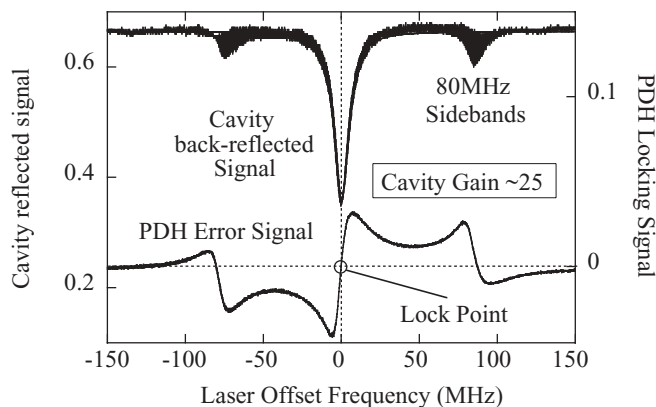

FIG. 3. Back-reflected cavity signal at 423 nm delivered to a fast photodiode using the optical fiber. The 80-MHz sidebands are generated by a resonant EOM. The PDH error signal is generated by mixing the 80-MHz local oscillator with the signal from the fast photodiode. This error signal is used to maintain the cavity on resonance (lock point) by adjusting the fast PZT driving the full reflector (mirror 2).
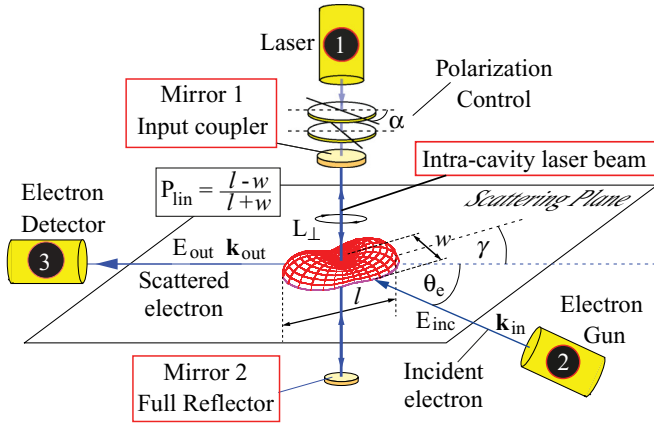
was altered using the piezo-controlled mirror. The main resonance at 0 MHz is accompanied by two sidebands at ±80 MHz, as required for the PDH locking technique. These sidebands are generated by passing the laser beam through an electro-optic modulator (EOM) resonant at this frequency. The back-reflected signal from the cavity that is focused into the fiber is detected by a fast photodiode whose output is mixed with the 80-MHz local oscillator to produce the PDH error signal. The output from the PDH electronics is then used to dynamically adjust the cavity length to ensure the enhancement cavity remains on-resonance with the laser beam when the cavity is locked.

The form of Eq. (1) can be used to estimate the cavity gain by monitoring the back-reflected signal from the passive cavity (i.e., when not locked to the laser) as a function of the laser offset frequency. For the mirrors chosen here, the theoretical maximum gain with no losses in the cavity is $G_{\mathrm{Cav}}^{SS(\mathrm{peak})} \sim 130$. In the example shown in Fig. 3, the calculated power gain inside the cavity was, however, ~25, measured with no atoms in the interaction region. This indicates additional intracavity losses $l_{IC}l_{FR}$ of ~4% were present, due either to scattering on the mirror surfaces or due to a slight misalignment of the cavity. This reduction in intracavity gain demonstrates how sensitive the enhancement is to any additional losses that are present.

Introduction of an atomic beam into the interaction region reduced the cavity gain from ~25 with no atomic beam to between 10 and 5, depending upon the beam density that was used. This indicates the total round-trip attenuation due to absorption and spontaneous emission in the atomic ensemble varied from $l_{\mathrm{tot}}^{SS} = l_2^{SS}l_4^{SS}l_6^{SS}l_8^{SS} = (l_2^{SS}l_4^{SS})^2 \sim 92\%$ for a gain of 10, to $l_{\mathrm{tot}}^{SS} \sim 84\%$ for a gain of 5.

The theoretical maximum gain for these atomic attenuation coefficients with no additional losses at the mirrors was ~25 and ~13, respectively, for optimized input couplers with $t_1^{\mathrm{match}} = 4\%$ and 8%. Since the input coupler used here had $t_1 \sim 3\%$, it is clear that maximum power was not being transmitted into the cavity during the current experiments. Future operation with the cavity will hence adopt custom-designed input couplers so as to maximize the intracavity field.

IV. EXPERIMENTAL RESULTS

Although the gain measured here is relatively low when the intracavity field is resonant with the atomic ensemble, this does not imply a degradation of the experiment, since the key goal is to produce a large excited-state population prior to superelastic electron collisions occurring. Since the reduction in cavity gain is directly related to the efficient creation of excited targets, it is instructive to consider the effect the laser cavity has on the superelastic data, since these provide a direct and sensitive probe of the 4^1P_1 substate populations and coherences produced by the field. Further, since the superelastic scattering measurements are directly related to the polarization state of the intracavity field, these data provide a highly sensitive probe of the field.

Figure 4 shows the superelastic scattering geometry adopted [2,4,5]. The laser beam passed through polarization-defining optics before entering the cavity. The radiation at the

FIG. 4. (Color online) The superelastic scattering process. The intracavity laser beam of wavelength λ excites the atoms via optical pumping. An incident electron of energy E_{inc} then de-excites the target and is detected with energy $E_{out} = E_{inc} + hc/\lambda$. P_{lin}, γ and $L_\perp$ derived from the superelastic signal describe the shape of the charge cloud.

interaction region creates excited calcium atoms in the 4^1P_1 state, whose shape is controlled by a set of optical pumping parameters related to the polarization of the intracavity field [8]. The incident electron de-excites the laser-prepared target and is scattered into the electron detector through an angle θ_e with respect to its initial momentum vector. The ACPs P_{lin}, γ then describe the target alignment, whereas $L_\perp$ defines the target orientation. Full details of these types of scattering processes can be found in [9].

A key advantage of using calcium as the target atom is that it has no hyperfine structure, and so all optical pumping parameters that define the laser-excited target are unity for radiation that is fully polarized. The ACPs determined from the superelastic scattering rates then provide a very sensitive and direct test of the intracavity field. Measurements with the cavity in place were hence directly compared to those obtained at 45 eV without the cavity [5], and it was found that the ACPs agreed over all measured angles, as shown in Fig. 5. *This demonstrates that the confocal cavity preserves the polarization of the incident laser beam, which is essential in these types of study.*

Further tests were carried out by reducing the laser power incident onto the cavity, and it was found that the superelastic signal could be obtained with good statistical accuracy for input powers as low as 5 mW. By comparison, results without the cavity typically use input powers in excess of 80 mW to obtain equivalent signal strengths. This clearly shows the advantage of using an enhancement cavity in experiments where only low laser power is available.

Figure 6 shows superelastic collision data for an electron energy $E_{out} = 100$ eV, taken with the enhancement cavity in operation. These data were obtained over a period of 2 weeks with an input power of 20 mW, the cavity remaining on resonance throughout this time. The data have high accuracy over the measured angular range $\theta_e = 8°–145°$ and reveal the complex variation in the ACPs as a function of θ_e typical in these experiments. At $\theta_e = 16°$ and $72°$ the collision produces a predominantly oriented target ($|L_\perp| \sim 1$); however, the
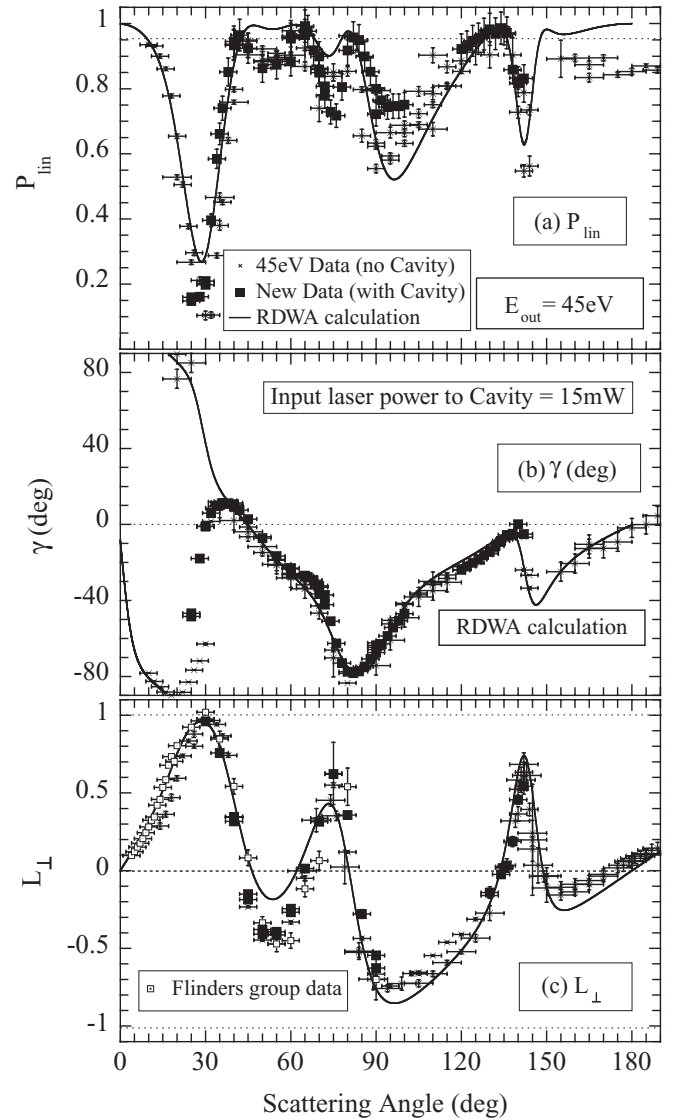

FIG. 5. $P_{lin}, \gamma, L_\perp$ derived from superelastic scattering with and without the enhancement cavity in operation, at an energy $E_{out} = 45$ eV. Data from experiments using the enhancement cavity with an input laser power of 15 mW (■) are directly compared to those without the cavity in place, which used an input power of $\sim$80 mW ($\times$) [4,5]. Excellent agreement is found between results for all measured scattering angles, showing that the polarization of the cavity field is the same as that of the incident laser beam. The RDW calculations of [10] are also shown as a comparison with experiment, as are results from the Flinders group [11] for $L_\perp$ ($\odot$).

direction of orientation is reversed. At θ_e from $30°$ to $60°$ and above $120°$ the state is almost fully aligned ($P_{lin} \sim 1$), the alignment angle γ being negative and varying only slowly. For other scattering angles the direction of the charge cloud changes rapidly, as does the shape.

The inset figures depict a representation of the charge cloud at selected angles, compared to the direction of the incident electron in a conventional coincidence measurement (i.e., opposite to the outgoing electron direction used here). These shapes were calculated as described in [2] and show the changes in the charge cloud as the ACPs vary with scattering angle.
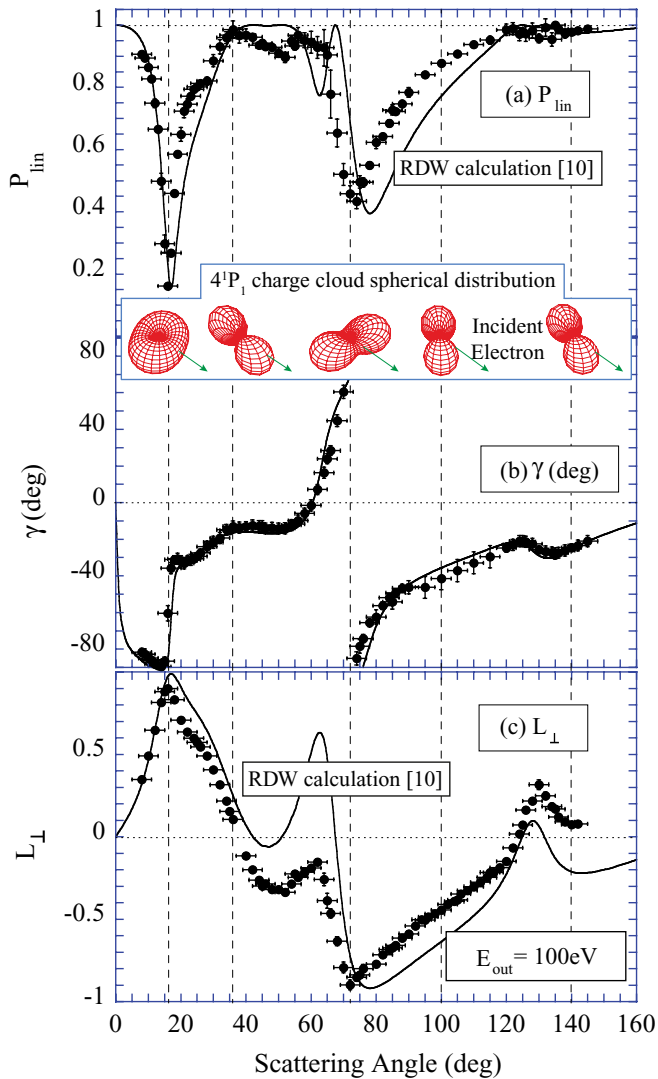
FIG. 6. (Color online) Measurements of the atomic collision parameters $P_{\text{lin}}, \gamma, L_\perp$ derived from superelastic scattering inside the resonant optical enhancement cavity, at an energy $E_{\text{out}} = 100$ eV. The inset shows the shape of the calculated charge cloud at selected angles, as derived from measurements. Unpublished RDW calculations kindly supplied by Chauhan and colleagues [10] are also shown.

Unpublished calculations at this energy were kindly provided by Professor Al Stauffer and Professor Rajesh Srivastava using their relativistic distorted wave (RDW) theory [10].

Comparison with the data indicates that the state alignment is well represented by theory. There is a small angular shift of the minimum in P_{lin} near $80°$; however, the magnitude is predicted well. The calculation for γ is remarkably accurate and passes through all data points (such excellent agreement is also observed at other energies for this target [4,5]). Comparison to theory for $L_\perp$ is less satisfactory. The calculation shows similar structure to the data, but the predicted peaks and troughs have different magnitudes. Since γ directly relates to the relative phase shift between the 4^1P_1 $m_J = \pm 1$ substate amplitudes, and $L_\perp, P_{\text{lin}}$ relate to their magnitudes, it appears the RDW theory is accurate in predicting the phase shifts but is less precise when calculating the substate amplitudes.

V. CONCLUSIONS

The results presented here clearly demonstrate that the adoption of a resonant enhancement cavity around an interaction region produces significant advantages, particularly in experiments where only low laser powers are available. Superelastic experiments provide a direct and very sensitive test of the effect of the intracavity field on the atomic ensemble, and the data taken here with the cavity in place show that high-precision measurements can be obtained for input powers less than 20% of that required without a cavity. The results further show that the intracavity field maintains the polarization of the input laser, and so this technique can be adopted in a much wider range of experiments, including atom trapping and the production of dipole traps. Further, since the intracavity power is often much greater than that of the input beam, it now becomes possible to study targets in higher Rydberg states using CW lasers, a research area that has almost exclusively used high-power pulsed lasers (with their associated low coherence) in the past. Experiments to study targets in these higher excited states are currently under consideration in Manchester. These will use these cavity enhancement techniques to provide superelastic scattering data from highly excited Rydberg targets.

[1] Layertec GmbH, http://www.layertec.com.

[2] A. J. Murray, W. R. MacGillivray, and M. Hussey, Phys. Rev. A **77**, 013409 (2008).

[3] A. J. Murray and M. Hussey (unpublished).

[4] M. Hussey, A. J. Murray, W. R. MacGillivray, and G. C. King, Phys. Rev. Lett. **99**, 133202 (2007).

[5] M. Hussey, A. J. Murray, W. R. MacGillivray, and G. C. King, J. Phys. B **41**, 055202 (2008).

[6] A. J. Murray, M. J. Hussey, and M. Needham, Meas. Sci. Technol. **17**, 3094 (2006).

[7] R. W. P. Drever, J. L. Hall, F. W. Kovalski, J. Hough, G. M. Ford, A. J. Munley, and H. Ward, Appl. Phys. B **31**, 97 (1983).

[8] P. M. Farrell, W. R. MacGillivray, and M. C. Standage, Phys. Rev. A **44**, 1828 (1991).

[9] N. Andersen, J. W. Gallagher, and I. V. Hertel, Phys. Rep. **165**, 1 (1988).

[10] R. J. Chauhan, R. Srivastava, and A. D. Stauffer, J. Phys. B **38**, 2385 (2005).

[11] M. R. Law and P. J. O. Teubner, J. Phys. B **28**, 2257 (1995).